JOURNAL OF GEOPHYSICAL RESEARCH, VOL. 113, D09202, doi:10.1029/2007JD009170, 2008

Direct aerosol forcing: Calculation from observables and sensitivities to inputs

Allison McComiskey,[1] Stephen E. Schwartz,[2] Beat Schmid,[3] Hong Guan,[4] Ernie R. Lewis,[2] Paul Ricchiazzi,[5] and John A. Ogren[6]

Received 13 July 2007; revised 11 October 2007; accepted 24 January 2008; published 7 May 2008.

[1] Understanding sources of uncertainty in aerosol direct radiative forcing (DRF), the difference in a given radiative flux component with and without aerosol, is essential to quantifying changes in Earth's radiation budget. We examine the uncertainty in DRF owing to measurement uncertainty in the quantities on which it depends: aerosol optical depth, single scattering albedo, asymmetry parameter, solar geometry, and surface albedo. Direct radiative forcing at the top of the atmosphere and at the surface is calculated at three locations representing distinct aerosol types and radiative environments. Sensitivities, the changes in DRF in response to unit changes in individual aerosol or surface properties, are also calculated for these conditions. The uncertainty in DRF associated with a given property is computed as the product of the sensitivity and typical measurement uncertainty in the respective property. Sensitivity and uncertainty values permit estimation of total uncertainty in calculated DRF and identification of properties that most limit accuracy in estimating forcing. Absolute total uncertainties in modeled local diurnally averaged forcing range from 0.2 to 3.1 W m^{-2} for the ranges of properties examined here. Relative total uncertainties range from ~20 to 80% with larger values at higher latitudes, where fluxes are low. The largest contributor to total uncertainty in DRF is single scattering albedo; however, decreasing measurement uncertainties for any property would increase accuracy in DRF. Comparison of two radiative transfer models suggests the contribution of modeling error is small compared to the total uncertainty although comparable to uncertainty arising from some individual properties.

Citation: McComiskey, A., S. E. Schwartz, B. Schmid, H. Guan, E. R. Lewis, P. Ricchiazzi, and J. A. Ogren (2008), Direct aerosol forcing: Calculation from observables and sensitivities to inputs, *J. Geophys. Res.*, *113*, D09202, doi:10.1029/2007JD009170.

1. Introduction

[2] Accurate knowledge of aerosol radiative forcing, the difference in net radiative flux at a given level in the atmosphere with and without aerosol, and of anthropogenic aerosol radiative forcing, the difference in net radiative flux with and without anthropogenic aerosol, is essential to understanding Earth's radiation budget and changes in this budget over the industrial period. Aerosol radiative forcings are generally classified as direct (forcing by scattering and absorption of radiation in cloud-free sky) and indirect (owing to influences of aerosols on the reflectivity and persistence of clouds). These forcings are highly variable in space and time; locally and instantaneously they can be tens of watts per square meter [*Charlson et al.*, 1992]. On a global average basis, the direct radiative forcing (DRF) at the top of the atmosphere (TOA) owing to anthropogenic aerosols is negative, offsetting to some extent a positive radiative forcing by enhanced greenhouse gases (GHGs) [*Charlson et al.*, 1990]. In contrast to GHGs, for which the concentrations, distributions, and radiative properties are relatively well known, the sources, lifetimes, and distributions of aerosols are highly variable, both spatially and temporally, making the effect of aerosols on climate difficult to quantify [e.g., *Anderson et al.*, 2003]. This difficulty is reflected, for example, in the range given for anthropogenic aerosol DRF in the work of *Intergovernmental Panel on Climate Change* (*IPCC*) [2007], $-0.5 + 0.4$ W m^{-2}. In this paper, we provide information to guide the systematic reduction of uncertainties in aerosol direct radiative forcing that result from the measurement uncertainty in aerosol and surface properties on which forcing depends.

[3] Calculation of aerosol DRF with a radiative transfer model for a given time and location depends on aerosol optical properties that are used as model inputs. The first-order aerosol properties affecting DRF as they are most commonly input into models are the aerosol optical depth,

[1] Cooperative Institute for Research in the Environmental Sciences, University of Colorado, Boulder, Colorado, USA.
[2] Atmospheric Sciences Division, Brookhaven National Laboratory, Upton, New York, USA.
[3] Pacific Northwest National Laboratory, Richland, Washington, USA.
[4] Bay Area Environmental Research Institute, Sonoma, California, USA.
[5] Institute for Computational Earth System Science, University of California, Santa Barbara, Santa Barbara, California, USA.
[6] NOAA Earth System Research Laboratory, Boulder, Colorado, USA.

0148-0227/08/2007JD009170$09.00

τ, the single scattering albedo, ω, the asymmetry parameter, g, and the wavelength dependencies of these quantities. Calculated DRF depends also on situational variables, importantly surface albedo, α, and its wavelength dependence, solar geometry, and also, weakly, on the vertical distribution of the aerosol. The uncertainty in calculated DRF reflects uncertainties in these input quantities and their wavelength dependencies. Additionally, there can be errors resulting from spatial and temporal variability of the properties in the environment that are not easily represented in the model, as well as inaccuracies in model physics.

[4] Here the contributions to uncertainty in DRF resulting from typical measurement uncertainties associated with each of the properties on which DRF depends are examined. A sensitivity, S_i, is computed as the change in DRF with respect to unit change in one of the aerosol or surface properties. S_i indicates the importance of an individual property in driving a change in forcing under particular conditions. An uncertainty, ΔF_i, the product of the sensitivity and its respective measurement uncertainty, is also computed for each of the aerosol and surface properties. Individual uncertainties are then combined into a total uncertainty, ΔF, in calculated DRF. The individual uncertainties indicate the impact of each variable on the total uncertainty and also permit the specification of how well these properties must be known in order to determine DRF, total anthropogenic forcing (aerosols plus gases), and climate sensitivity to a desired accuracy.

[5] The motivation for quantifying uncertainties in DRF associated with τ, ω, g, and α is to guide efforts in improving measurement of these quantities and modeling that will reduce uncertainty in calculated aerosol radiative effects. The calculations presented here are intended to broadly define the range of uncertainty that results from a range of input variables commonly used for modeling DRF globally and to identify which measurements most limit accuracy in its estimation. We have also established a framework from which the uncertainty in DRF can be determined for any specific set of conditions (e.g., a field campaign or specific region) given a set on input parameters. By using different radiative transfer models, the contribution of different model approaches to uncertainties in DRF calculations is examined.

2. Aerosol Direct Radiative Forcing

[6] It is now generally recognized that as a consequence of industrial practices increased aerosol concentrations exert a substantial radiative effect on Earth's climate. Early estimates of the global mean direct radiative forcing at the TOA based on simple analytical formulas, which assumed canonical values for aerosol optical properties, ranged from ~ -0.6 to -1.0 W m^{-2} for anthropogenically produced sulfate aerosol [*Charlson et al.*, 1991, 1992] to ~ -1.0 W m^{-2} for biomass burning aerosol [*Penner et al.*, 1992]. These estimates suggested that clear-sky aerosol could force a global-mean cooling of magnitude similar to the warming forced by enhanced concentrations of GHGs, necessitating inclusion of clear-sky aerosol forcing in climate models. However, the uncertainties given to these estimates were each about a factor of two. *Penner et al.* [1994] refined uncertainty estimates for sulfate with an uncertainty factor of 2.3 for a forcing of -0.6 W m^{-2}, and biomass burning with an uncertainty factor of 2.7 with a forcing of -0.86 W m^{-2}, detailing individual factors contributing to the total uncertainty, principally emissions, lifetimes, and optical properties. The investigators stressed that estimating uncertainties was possible only for these well-known species but not for other anthropogenic aerosol species.

[7] Subsequently, estimates such as these for purely scattering aerosols were extended to include absorbing aerosols. *Chylek and Wong* [1995] showed that the range in size distribution of absorbing biomass burning aerosol expected globally could result in a range of forcing from -0.2 to -1.1 W m^{-2}. Taking into account the absorbing properties of fossil fuel burning aerosol, *Haywood and Shine* [1995] calculated a positive forcing owing to soot of between 0.04 and 0.18 W m^{-2}, with uncertainties caused by unknown geographical distributions of the aerosol and assumptions regarding aerosol optical properties. However, the warming contribution owing to absorbing aerosols could reduce the magnitude of the estimated aerosol direct forcing by up to 40%. *Russell et al.* [1997] further extended these simple formulas to account for the dependence on solar zenith angle of radiation interactions in the atmosphere and with the surface. Results from this expression compared within a few watts per square meter with results from more complex radiative transfer models [*Russell et al.*, 1997; *Redemann et al.*, 2000], with larger uncertainties at very high and very low solar angles. Such expressions are efficient and useful for determining forcing at the regional scale where optical depths and forcing are larger than global averages. However, *Redemann et al.* [2000] found that using a detailed radiative transfer model and vertical profiles of measurements, details in the vertical dimension of aerosol radiative forcing could be resolved, illustrating the need for more comprehensive measurements of spatially resolved aerosol properties in combination with more complex models.

[8] An extensive intercomparison of the radiative forcing by nonabsorbing sulfate aerosols calculated by several radiative transfer models for a broad range of aerosol and environmental conditions [*Boucher et al.*, 1998] found that the relative standard deviation of the zenith-angle-average broadband forcing for 15 models was 8% for particle radius near the maximum in this forcing (ca. 200 nm) and at low surface albedo. Somewhat greater model-to-model discrepancies were exhibited at specific solar zenith angles. Still greater discrepancies were exhibited at smaller particle radii, and much greater discrepancies at high surface albedos, at which the forcing changed sign; in these situations, however, the forcing was quite small. The discrepancies were attributed to differences in the treatment of Mie scattering, multiple scattering, phase functions, and spectral and angular model resolution. However, the uncertainty in forcing caused by errors in treatment of the radiative transfer was small compared to uncertainty in forcing from poorly defined aerosol properties. A more extensive study by *Halthore et al.* [2005] found substantial model-to-model differences in TOA forcing that depended on solar zenith angle and aerosol optical depth. At solar zenith angle $\theta = 75°$ the relative standard deviation in forcing for 16 models ranged from 5 to 13% but at $\theta = 30°$ the relative standard deviation in forcing was much greater, ranging from 27 to

62%, with some models even differing in sign, despite well specified aerosol properties and low surface reflectance (0.2).

[9] The accuracy of radiative transfer models used in computing aerosol radiative effects has been tested against measured radiation at the surface in so-called closure studies. Some studies involving comparisons of several radiative transfer models found that the diffuse radiation component was greatly overestimated by models when compared to measurements; this overestimation was too great to be explained by measurement uncertainties [*Kato et al.*, 1997; *Halthore and Schwartz*, 2000; *Halthore et al.*, 2005], and the causes for the overestimation have not been fully identified. A recent closure experiment using data from the Department of Energy (DOE) Atmospheric Radiation Measurement (ARM) Program site in north central Oklahoma [*Michalsky et al.*, 2006] showed six different models agreed to within 1% for measured direct irradiance and to within 1.9% for measured diffuse irradiance. The use of highly controlled observations of aerosol optical properties in this study suggests the importance of accurate model inputs when computing aerosol radiative forcing. Improved estimates of aerosol direct forcing require improvements in specification of aerosol properties and their spatial and temporal distribution, in the attribution to sources for anthropogenic forcing, and in treatment of the radiative transfer.

[10] In an effort to gain improved global estimates of aerosol direct forcing, and especially of anthropogenic aerosol direct forcing, chemical transport models (CTM) have been employed as reviewed in IPCC AR3 [*Penner et al.*, 2001, chap. 5], and AR4 [*Forster et al.*, 2007, chap. 2]. Such estimates of radiative forcing have depended on emissions data and chemical transport models to distribute the aerosol geographically. A strength of this approach is that it can account for geographical and temporal distribution of aerosols by transporting, evolving, and removing aerosols and precursor gases. Because of the variable sources of anthropogenic aerosols (primary and secondary), the multiple chemical species that comprise these aerosols, and their variable and evolving size distributions (including short-range temporal and spatial variability owing to uptake of water by hygroscopic particles), the optical properties affecting their radiative influence are highly variable and difficult to model or to generalize from limited measurements. The primary modeled quantity is aerosol mass loading, with inputs to radiation calculations for aerosol properties such as mass scattering efficiency (leading to aerosol optical depth), upscatter fraction, single scattering albedo, and environmental properties such as surface albedo being based on assumptions and empirical estimates.

[11] The large uncertainty in present estimates of anthropogenic aerosol direct radiative forcing inferred by the use of CTMs is thus due both to uncertainty in the amount and geographical distribution of anthropogenic aerosol and to uncertainty in aerosol optical properties and situational variables influencing the radiative transfer. An intercomparison of forcing by several global chemical transport models undertaken by the AeroCom initiative showed that the primary driver of variability in the forcing was the variability in forcing per-unit aerosol optical depth [*Schulz et al.*, 2006], a quantity that is dependent on the difference in aerosol optical properties such as ω and g, rather than aerosol amount. *Bates et al.* [2006] assessed two different chemical transport models in three oceanic regions, using observations from three comprehensive field campaigns downwind of large population centers and aerosol source regions to constrain estimates of DRF and provide comparisons to model-based estimates. Model estimates that did not use observations to constrain the computation, but instead used parameterizations from *IPCC* [2001], exhibited uncertainties approximately 25% higher than the constrained estimates. However, even the constrained estimates from CTMs showed substantial differences in aerosol amount compared to measurements. Confidence in this approach requires extensive validation through global long-term monitoring of the relevant variables.

[12] An alternative approach to estimating aerosol direct forcing relies primarily on observations. Over the past several years, measurement-based estimates of the aerosol direct radiative forcing have become possible through field campaigns, long-term observational programs, and improvements in measurements of aerosol and environmental properties. *Bergstrom and Russell* [1999] estimated regional aerosol radiative forcing from in situ aerosol properties observed during the TARFOX campaign and satellite-based aerosol optical depths from the Advanced Very High-Resolution Radiometer (AVHRR). These regional estimates compared well with results from some global models for the same region, and discrepancies with other model results were attributed to unknown inputs for the model concerning regional distribution of aerosol types and their properties. Global distributions of aerosol optical depth and its wavelength dependence derived from satellite observations together with representative aerosol optical properties derived from nearby surface measurements from AERONET (Aerosol Robotic Network; *Dubovik and King* [2000]) were used by *Bellouin et al.* [2005] to infer anthropogenic direct aerosol forcing at the top of the atmosphere, and accounting for cloud fraction, as -0.8 ± 0.1 W m^{-2}.

[13] Because of the high spatial and temporal variability of aerosol loading and properties such an approach requires space-based observations and/or a dense network of surface observations. Where observations are lacking, a combination of observations and CTMs to distribute aerosol can be exploited. Using various satellite- and ground-based data to compute aerosol radiative effects over land and ocean, and chemical transport models to distribute aerosol geographically over land, *Yu et al.* [2006] showed the local instantaneous broadband shortwave TOA forcing to be -5.5 ± 0.2 W m^{-2} over ocean and -4.9 ± 0.7 W m^{-2} over land. Model-based estimates for the same scenarios were $\sim$30–40% lower than the observationally based estimates. The investigators cited a lack of sufficient observations for aerosol properties (primarily absorption) and surface reflectance, especially on regional scales, as the primary contributors to uncertainty in using observations to calculate the forcing.

[14] A further consideration with respect to evaluation of aerosol direct radiative forcing is that observations of aerosol properties made by different instruments and techniques and from different platforms can differ widely depending on measurement approach. Each approach has

its own uncertainties that are sometimes difficult to quantify. Ground-based in situ observations (e.g., NOAA Earth Systems Research Laboratory (ESRL); *Delene and Ogren* [2002]) typically include aerosol light scattering in the forward and backward direction and light absorption. These direct measurements can be used to derive optical properties, such as ω and g, that can be input into radiative transfer models. Ground-based in situ measurements are representative of near-surface aerosol. Information on the aerosol vertical profile can be obtained with surface-based, airborne, or space-borne lidars, and with aircraft in situ and remote sensing measurements [*Schmid et al.*, 2006, and references therein]. Airborne observations of atmospheric transmittance and upwelling and downwelling fluxes have been used to measure instantaneous aerosol radiative forcing efficiency directly [*Redemann et al.*, 2006].

[15] Ground-based remote sensing networks (e.g., AERONET; *Holben et al.* [1998]; MultiFilter Rotating Shadowband Radiometer, MFRSR; *Harrison et al.* [1994]) measure direct solar irradiance at specific wavelengths, from which aerosol optical depth and other aerosol properties can be derived for the entire atmospheric column when clouds are not present. More complex retrievals provide values of ω and g that are also representative of the aerosol in the column above the measurement site [e.g., *Dubovik and King*, 2000; *Kassianov et al.*, 2005]. Satellite sensors such as the Moderate Resolution Imaging Spectroradiometer (MODIS) and Multiangle Imaging SpectroRadiometer (MISR) can provide global information on columnar aerosol optical properties [e.g., *Russell et al.*, 2007] but only under noncloudy conditions. Retrieval of aerosol properties from space over the oceans come with a high degree of confidence [e.g., *Wagener et al.*, 1997], but retrievals over more highly reflecting land surfaces can carry larger uncertainties. Comprehensive validation of remote sensing retrievals of aerosol properties using in situ measurements are still required.

[16] In summary, although methods of calculating the aerosol direct radiative forcing have evolved greatly, and although the associated uncertainties have been reduced, these uncertainties are still high relative to the magnitude of the forcing and relative to uncertainties associated with the better understood forcing by GHGs. The first attempts at estimating uncertainties were global averages using simple formulas and assumed values for aerosol properties [e.g., *Charlson et al.*, 1991, 1992]. Here we address the portion of that uncertainty due specifically to uncertainty in measurements at a local scale and for a range of possible conditions. Efforts to reduce measurement uncertainties are the key to providing an estimate of the aerosol direct radiative forcing with uncertainty sufficiently low that it can be used, for example, to evaluate the performance of climate models over the industrial period [*Schwartz*, 2004].

3. Approach

3.1. Sensitivity and Uncertainty of Forcing

[17] Aerosol direct radiative forcing, F, is evaluated either at the top of the atmosphere (TOA) or at the surface (SRF), as

$$F = (f_a\downarrow - f_a\uparrow) - (f_0\downarrow - f_0\uparrow), \quad (1)$$

Table 1. Range Over Which Aerosol Properties Are Varied for Calculations of Forcings and Uncertainties Used in the Calculation of S_i and ΔF[a]

Property p_i	Range	Uncertainty Δp_i
$\tau(0.55)$	0.0–0.3	0.01
$\omega(0.55)$	0.75–1.00	0.03
$g(0.55)$	0.50–0.75	0.05
α_{UVV}	0.0–1.0	0.05
α_{SIR}	0.0–1.0	0.05

[a]These uncertainties are estimates that are representative of current measurement approaches.

where f denotes the irradiance (downwelling or upwelling, W m^{-2}) or spectral irradiance (W m^{-2} μm^{-1}) and ($f\downarrow - f\uparrow$) denotes the net irradiance (downwelling minus upwelling) computed with a given aerosol, f_a, or without aerosol, f_0, at either the TOA or SRF.

[18] As DRF can be calculated in many different forms; in an average sense globally, annually, or diurnally versus instantaneously, or integrated over a broad spectral range versus at a single wavelength, we selected three different radiative forcing quantities for analysis: (1) the forcing integrated over the solar spectrum (0.25–4.0 μm) and averaged over solar zenith angle for 24 hours at the equinox, $\overline{F_S}$, (W m^{-2}); (2) the forcing of spectral irradiance at 0.55 μm, likewise averaged over solar zenith angle for 24 hours at the equinox, $\overline{F_{0.55}}$, (W m^{-2} μm^{-1}); and (3) the instantaneous forcing integrated over the solar spectrum at a specific solar zenith angle θ, $F_S(\theta)$, (W m^{-2}).

[19] To determine the total uncertainty in each of the several forcings that is due to the uncertainty in the properties on which it depends, we examine the dependence of F on each property, τ, ω, g, and α, in isolation. For the purpose of determining the dependence of F on surface albedo, α is held as a constant in two separate wavelength ranges: the ultraviolet-visible (α_{UVV}), 0.25–0.75 μm, and the shortwave-infrared (α_{SIR}), 0.75–4.0 μm. F is calculated for a range of values for each of these input quantities, given in Table 1, that incorporates the bulk of values observed for these properties globally.

[20] The sensitivity of each forcing quantity to each of the individual aerosol and environmental properties of interest is defined as

$$S_i = \frac{\partial F}{\partial p_i}, \quad (2)$$

where p_i is the value of the aerosol or environmental property of interest. The uncertainty in F owing to each of the individual aerosol and environmental properties is then given by

$$\Delta F_i = S_i \Delta p_i, \quad (3)$$

where Δp_i is the uncertainty in the given property. For the F values presented in section 5, ΔF_i can be calculated for any known measurement uncertainty of interest. Uncertainties used here (Table 1) are typical for commonly used measurements. Values of S_i presented in this paper represent the change

in F per-unit change in the controlling property p_i; values of ΔF_i represent the change in F per assumed change in p_i.

[21] The total uncertainty in forcing, ΔF, owing to the combined influence of the uncertainties in the several input quantities is determined under the assumption that these uncertainties are uncorrelated as:

$$\Delta F = \sum\nolimits^{\oplus} \Delta F_i, \tag{4}$$

where the notation $\sum^{\oplus}$ denotes summation in quadrature, i.e., $\sum^{\oplus} x_i \equiv (\Sigma x_i^2)^{1/2}$, and for this study specifically:

$$\Delta F = \left[\left(\frac{\partial F}{\partial \tau}\Delta\tau\right)^2 + \left(\frac{\partial F}{\partial \omega}\Delta\omega\right)^2 + \left(\frac{\partial F}{\partial g}\Delta g\right)^2 + \left(\frac{\partial F}{\partial \alpha_{UVV}}\Delta\alpha_{UVV}\right)^2 + \left(\frac{\partial F}{\partial \alpha_{SIR}}\Delta\alpha_{SIR}\right)^2 \right]^{1/2}. \tag{5}$$

Correlation in the variation among these properties has been shown to be significant in some cases [e.g., *Anderson et al.*, 1999], which may increase the actual uncertainty in DRF. Here, however the uncertainties are treated as if they are uncorrelated. We use ΔF to present the variation in magnitude of the fractional uncertainties for different locations and radiative environments but the absolute total uncertainties presented here must be considered in light of this assumption. Each of the quantities presented in equations (1)–(5) maintains the units of the corresponding forcing, W m^{-2} (or W m^{-2} μm^{-1}), and can therefore be directly compared to that forcing.

[22] The primary influence on each of the forcings is τ; as τ varies, the contribution of each of the other properties to ΔF will also vary. The sensitivity of F to τ can also be expressed in terms of the radiative forcing efficiency, ε, the forcing per-unit aerosol optical depth: $\varepsilon = F/\tau$. Uncertainty in F gives loading-dependent uncertainty that is likely dominated by τ, and uncertainty in ε gives the uncertainty owing to the other optical properties. Sensitivity of ε to aerosol properties is important as ε is often used to estimate F in situations for which aerosol optical depth is available, from ground- or space-based remote sensing measurements, but for which other aerosol properties are not well known [e.g., *Anderson et al.*, 2005]. ε is easily derived from values of F provided here and can then be used to determine F or its sensitivities for any given τ. Equations (3)–(5) can also be modified to provide the total uncertainty in the radiative forcing efficiency, $\Delta\varepsilon$, by substituting ε for F.

3.2. Modeled Radiative Environments

[23] To examine sensitivities, we selected base cases that represent typical conditions for three radiative environments and aerosol types. Typical aerosol and surface conditions for these base cases were taken from three sites maintained long term by the ARM Program (http://www.arm.gov): Nauru in the Tropical Western Pacific (TWP) (0.52°N), north central Oklahoma in the Southern Great Plains (SGP) (36.61°N), and the North Slope of Alaska (NSA) (71.32°N). The modeled values of the forcings were found to differ greatly among the several cases examined as differences in location and time result in differences in solar geometry and in aerosol and surface properties.

Table 2. Properties Chosen for the Base Cases

	TWP, 0.52°N Latitude	SGP, 36.61°N Latitude	NSA, 71.32°N Latitude
$\tau(0.55)$	0.05	0.1	0.05
$\omega(0.55)$	0.97	0.95	0.95
$g(0.55)$	0.8	0.6	0.7
$\mathring{a}_{sp}$	0.5	1.0	1.5
$\mathring{a}_{ap}$	1.0	1.0	1.0
α_{UVV}	0.05	0.1	0.9
α_{SIR}	0.05	0.4	0.8
λ_g, μm	5.0	5.0	5.0
θ	30°	45°	70°

[24] The base cases are defined by the properties in Table 2. The defined properties include τ, ω, and g at 0.55 μm; α_{UVV} and α_{SIR}; θ for calculations of instantaneous radiative forcing quantities ($F_S(\theta)$); the Ångström exponents for scattering, $\mathring{a}_{sp}$, and absorption, $\mathring{a}_{ap}$, as well as λ_g, the wavelength characterizing the transition from the Rayleigh regime to the Mie regime. Ångström exponents and λ_g are used in wavelength dependence parameterizations discussed in the next section. These values reflect a typical aerosol that would be expected at these sites and are not a direct result of measurements. The aerosol assigned to TWP has a relatively low aerosol optical depth, high single scattering albedo, and large asymmetry parameter characteristic of marine aerosol. The background continental aerosol assigned to SGP has a higher aerosol optical depth, lower single scattering albedo, and lower asymmetry parameter reflecting the smaller particles found at SGP. The aerosol assigned to NSA, representing Arctic haze, has similar properties to that at SGP with a lower aerosol optical depth and slightly higher asymmetry parameter. Ångström exponents for scattering and absorption are chosen to reflect the wavelength dependence that would be expected from aerosols with these properties (discussed in the following section). The surface albedo at TWP corresponds to an ocean surface with very low reflectivity that is flat throughout the spectral range. The vegetated surface at SGP has a lower reflectivity in the UVV portion of the spectrum and is higher in the SIR because of the greater near-IR reflectance of the leafy material. At NSA, the surface is assumed to be snow covered with a reflectance that is high in the UVV but slightly lower in the SIR because of increased absorption by ice. While F is calculated over the range of properties presented in Table 1, values of F, sensitivities, uncertainties, and model comparisons for the set of base case properties at each site are used for presenting results.

[25] The three forcing quantities defined above were each examined for each base case. These three forcing quantities were selected to be represented at different locations globally (Table 2). $\overline{F_S}$, which provides values that incorporate the full solar spectrum and a diurnal average for the equinox when solar positioning is neutral for the northern or southern hemisphere, is analogous to globally averaged or other calculations averaged over space and time. The spectral forcing $\overline{F_{0.55}}$ is suitable for consideration of radiative flux in narrow wavelength bands in the midvisible for which measurements with specific instruments and closure experiments are common. The instantaneous broadband forcing $F_S(\theta)$ is useful for consideration of instantaneous measurements and calculations at specific values of θ.

[26] Comparison of the sensitivities of the several forcing quantities provides an opportunity to differentiate the influences of averaged versus instantaneous or single wavelength conditions. For example, is the sensitivity to a particular property low because a strong dependence on wavelength or solar geometry has been diminished by averaging? If so, a stronger sensitivity will be seen in the spectral or instantaneous calculations. If the magnitude of the forcing for a given scenario or set of properties varies considerably from an averaged case the associated uncertainties will also vary accordingly.

3.3. Wavelength Dependence of Aerosol and Surface Properties

[27] Calculations of broadband aerosol forcing require the specification of aerosol optical and surface properties across the wavelength range of interest. Systematic spectral measurements of aerosol properties in the shortwave are rarely made, and the wavelength dependence of these properties in large portions of the spectrum is thus not well known. Typically, measurements are made at only a few wavelengths in the visible and near-infrared portions of the spectrum (e.g., NASA AERONET, NOAA ESRL, MODIS) and the wavelength dependence is interpolated and/or extrapolated throughout the shortwave on the basis of behavior at these observed wavelengths.

[28] Here we have adopted a parameterization for the wavelength dependence of the aerosol optical depth and single scattering albedo according to $\mathring{a}_{sp}$ and $\mathring{a}_{ap}$ given in Table 2. These exponents provide a power law scaling that results in the Ångström law for the wavelength dependence of aerosol optical depth and a physical value (between zero and one) for the single scattering albedo. Ångström exponents are applied such that an aerosol optical depth and single scattering albedo are calculated for 38 distinct wavelengths between 0.25 and 4.0 μm as

$$\tau(\lambda) = \tau(0.55)\left\{\left(\frac{0.55}{\lambda}\right)^{\mathring{a}_{sp}}\omega(0.55) + \left(\frac{0.55}{\lambda}\right)^{\mathring{a}_{ap}}[1-\omega(0.55)]\right\} \quad (6)$$

and

$$\omega(\lambda) = \frac{\left(\frac{0.55}{\lambda}\right)^{\mathring{a}_{sp}}\omega(0.55)}{\left(\frac{0.55}{\lambda}\right)^{\mathring{a}_{sp}}\omega(0.55) + \left(\frac{0.55}{\lambda}\right)^{\mathring{a}_{ap}}[1-\omega(0.55)]}. \quad (7)$$

[29] The asymmetry parameter is also calculated at 38 wavelengths over the range 0.25–4.0 μm by

$$g(\lambda) = g(0.55)\frac{1+\left(\frac{0.55}{\lambda_g}\right)^2}{1+\left(\frac{\lambda}{\lambda_g}\right)^2}, \quad (8)$$

where λ_g is chosen somewhat arbitrarily to be 5.0 μm. While the specific parameterization is not critically important to the results presented here, this expression yields physically reasonable asymptotic values when the size parameter ($x = 2\pi r/\lambda$ where r is the particle radius) is very large (Mie limit) or very small (Rayleigh limit). The wavelength dependencies of τ, ω, and g for the three base cases are shown in Figure 1. Also shown in the top panel for reference is the TOA incident solar radiation.

[30] Surface albedo is parameterized as a constant in two separate regions of the solar spectrum as:

$$\alpha(\lambda < 0.75\,\mu\text{m}) \equiv \alpha_{UVV} \quad (9)$$

and

$$\alpha(\lambda > 0.75\,\mu\text{m}) \equiv \alpha_{SIR} \quad (10)$$

[31] This division of the solar spectrum at 0.75 μm accounts for the distinct change in reflectance over vegetated and snow covered surfaces that occurs between the visible and near-IR wavelengths.

4. Radiative Transfer Models

[32] The calculations described above were made with two radiative transfer models, the Santa Barbara DISORT Atmospheric Radiative Transfer model (SBDART; *Ricchiazzi et al.* [1998]) and the Rapid Radiative Transfer Model Shortwave (RRTM_SW; *Clough et al.* [2004]). The model differences are used to infer the contribution of modeling errors to uncertainty in calculated forcings, and the magnitude of this contribution is compared to that owing to measurement uncertainties. Both models were included in a closure and model intercomparison project for the 2003 ARM Aerosol Intensive Observation Period [*Michalsky et al.*, 2006] in which an array of continuous, high-quality measurements made at the SGP site during this period provided aerosol properties and surface radiation measurements. All models obtained closure within 1% of measurements for direct irradiances and within 1.9% of measurements for diffuse irradiances at the surface, as noted above.

[33] SBDART and RRTM both use the Discrete Ordinate Radiative Transfer (DISORT) integration of the radiative transfer equation [*Stamnes et al.*, 1988]. The input and configuration parameters for this study were chosen to be identical for the two models to the extent possible. Calculations were made with eight streams in the wavelength range 0.25–4.0 μm using the *Gueymard* [2004] solar spectrum (Figure 1). The Henyey-Greenstein phase function was employed to calculate upscatter fraction from backscatter fraction. The vertical distribution of aerosol extinction (scattering plus absorption) is given in Figure 2. For SBDART the local extinction coefficient is constant within each of 33 layers up to 100 km, and in RRTM the local extinction coefficient is constant within each of five layers between 0 and 3 km. The contribution to the optical depth from aerosol above height z is shown in Figure 2 (this contribution is given as the integral from z to TOA of the aerosol extinction coefficient; the integral over the entire column is equal to τ). While the vertical profiles of extinction differ between SBDART and RRTM, the total column aerosol optical depths are the same in the two models. The vertical profile is of secondary importance

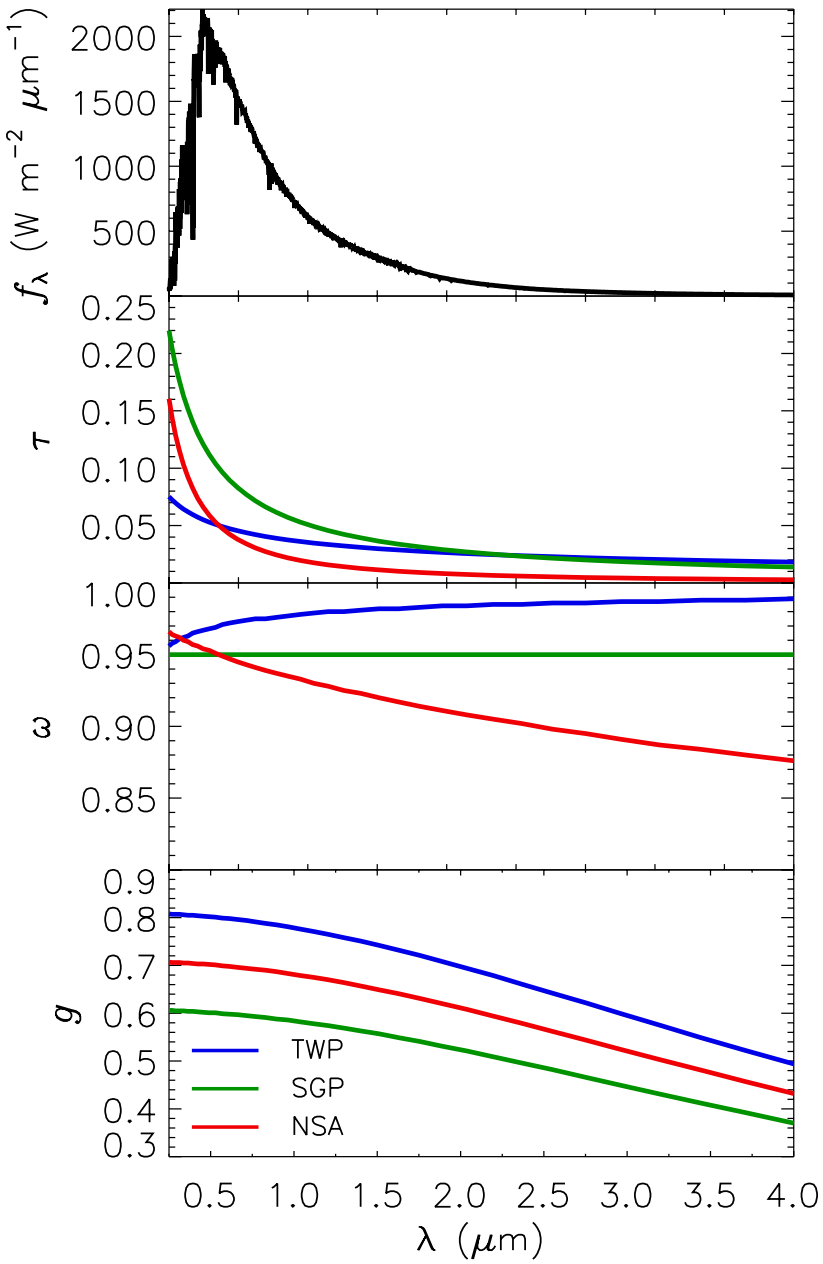

Figure 1. Dependence of aerosol optical properties optical depth, τ; single scattering albedo, ω; and asymmetry parameter, g, on wavelength, λ, for the three base cases. The top panel shows the TOA solar irradiance from *Gueymard* [2004].

for calculations of F at the TOA and SRF, especially for aerosols with low absorption [*Schmid et al.*, 2007].

[34] For each site, the standard atmospheres of *McClatchey et al.* [1972] were used to specify profiles of atmospheric temperature, pressure, and gas concentrations in the column for both models. Surface temperatures and column-integrated concentrations of primary gases are shown in Table 3. Pressure at the surface is 1013 hPa for each atmosphere. Cloud-free sky was assumed for all calculations. Radiative fluxes vary among the sites according to the profiles for each standard atmosphere but are the same at each site for the two models.

[35] The two radiative transfer models, as they are used here, differ primarily in their spectral resolution. While the resolution in SBDART can be modified by the user, the results here were produced by running the model with a wavelength increment of 0.005 μm. To reduce the time required for model runs, RRTM uses correlated-k distributions to create 14 bands in the shortwave in which the model is run without sacrificing accuracy in broadband calculations. For the wavelength range examined here, RRTM was run in 13 of its 14 bands, with each band ranging from approximately 0.06 to 0.77 μm in width. The spectral resolution of RRTM precludes a comparison with SBDART

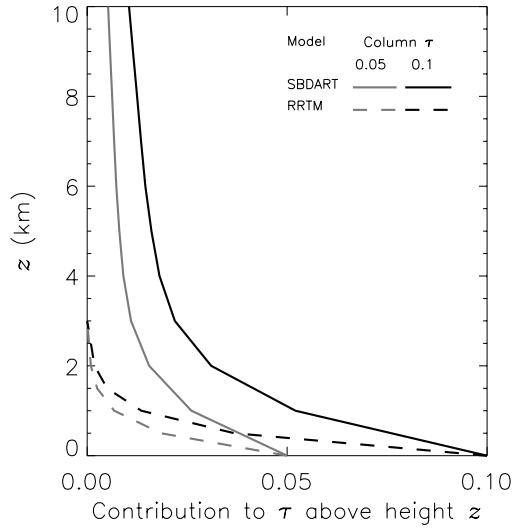

Figure 2. Contribution to the aerosol optical depth, τ, from aerosol above height, z, for SBDART and RRTM calculations for the two values of τ considered.

for $\overline{F_{0.55}}$, for which calculations are made at a single wavelength. The calculations that vary surface albedo are split between two broad wavelength ranges at 0.75 μm. Because a break in RRTM bands does not fall at 0.75 μm these calculations are also made only with SBDART.

[36] In addition to the two full radiative transfer models, we also evaluated instantaneous forcing and sensitivities calculated with a simple analytical expression. This expression, as presented by *Charlson et al.* [1991, 1992] for the direct aerosol radiative forcing F at TOA owing to scattering by aerosols for cloud-free sky and as modified by *Haywood and Shine* [1995] and *Chylek and Wong* [1995] to account for aerosol absorption,

$$F = -S_0 T_{\mathrm{atm}}^2 \tau \Big[(1-\alpha)^2 \omega\beta - 2\alpha(1-\omega)\Big], \qquad (11)$$

is valid for aerosol optical depth $\tau \ll 1$; S_0 is the solar constant ($\sim$1365 W m^{-2}), T_{atm} the atmospheric transmittance above the aerosol layer (the difference from unity being due to Rayleigh scattering and absorption by ozone and other gases), and β the upscatter fraction. The dependence of F on solar zenith angle θ is contained only in the atmospheric transmittance and in the upscatter fraction. The first term in the brackets is the negative forcing (cooling) owing to upscatter, whereas the second term is the positive forcing (heating) owing to absorption by aerosols. F can thus be either negative or positive, depending on the relative importance of the two terms in the brackets, this being determined by whether ω is greater or less than, respectively, a critical value given by

$$\omega_c = \frac{2\alpha}{(1-\alpha)^2\beta + 2\alpha} \qquad (12)$$

[cf. *Haywood and Shine*, 1995, Figure 1].

[37] Equation (11) allows calculation of other quantities of interest, specifically the sensitivities of F to the controlling properties τ, ω, g, and α:

$$\frac{\partial F}{\partial \tau} = -S_0 T_{\mathrm{atm}}^2 \Big[(1-\alpha)^2\beta\omega - 2\alpha(1-\omega)\Big], \qquad (13)$$

$$\frac{\partial F}{\partial \omega} = -S_0 T_{\mathrm{atm}}^2 \tau \Big[(1-\alpha)^2\beta + 2\alpha\Big], \qquad (14)$$

$$\frac{\partial F}{\partial g} = -S_0 T_{\mathrm{atm}}^2 \tau \Big[(1-\alpha)^2\omega\Big] \frac{\partial\beta}{\partial g}, \qquad (15)$$

and

$$\frac{\partial F}{\partial \alpha} = 2S_0 T_{\mathrm{atm}}^2 \tau[(1-\alpha)\beta\omega + (1-\omega)]. \qquad (16)$$

[38] In contrast to the forcing, which can be either positive or negative, $\partial F/\partial\omega$ is always negative, and $\partial F/\partial g$ and $\partial F/\partial\alpha$ are always positive (because $\partial\beta/\partial g < 0$).

5. Results and Discussion

[39] The direct aerosol radiative forcings, $\overline{F_S}$, $\overline{F_{0.55}}$, and and $F_S(\theta)$, and their associated sensitivities, uncertainties, and model differences are presented in this section. Graphical and tabular summaries of these quantities are given here for both models over the range of properties examined and for the base cases, as well as absolute and percent model differences. These summaries provide sufficient information for discussion, however, the full set of model calculations may be useful to investigators interested in uncertainty calculations pertinent to specific measurements. For this purpose, we have made available the full set of calculations at http://www.arm.gov. This database includes direct radiative forcing as well as radiative forcing efficiency calculated from both models for each of the three locations and radiative quantities.

5.1. Sensitivity of Forcing

[40] The forcing quantities $\overline{F_S}$, $\overline{F_{0.55}}$, and $F_S(\theta)$ differ substantially among the three locations for which the calculations were carried out both in their magnitudes and in their sensitivities to controlling properties as given by the slopes in the graphs presented in Figures 3a–3c. At both the top of the atmosphere and the surface, each quantity varies nearly linearly with each of the aerosol optical properties for the conditions examined here, so the sensitivity of a given

Table 3. Standard Atmospheres Used in Modeling the Three Base Cases, Surface Temperatures, and Integrated Column Concentrations of Absorbing Gases

Case	Standard Atmosphere	Surface Temperature, K	H_2O Vapor, g cm^{-2}	Total O_3, atm cm	O_3 Below 10 km, atm cm
TWP	tropical	300	4.12	0.25	0.022
SGP	US62	288	1.42	0.35	0.025
NSA	subarctic winter	257	0.42	0.49	0.034

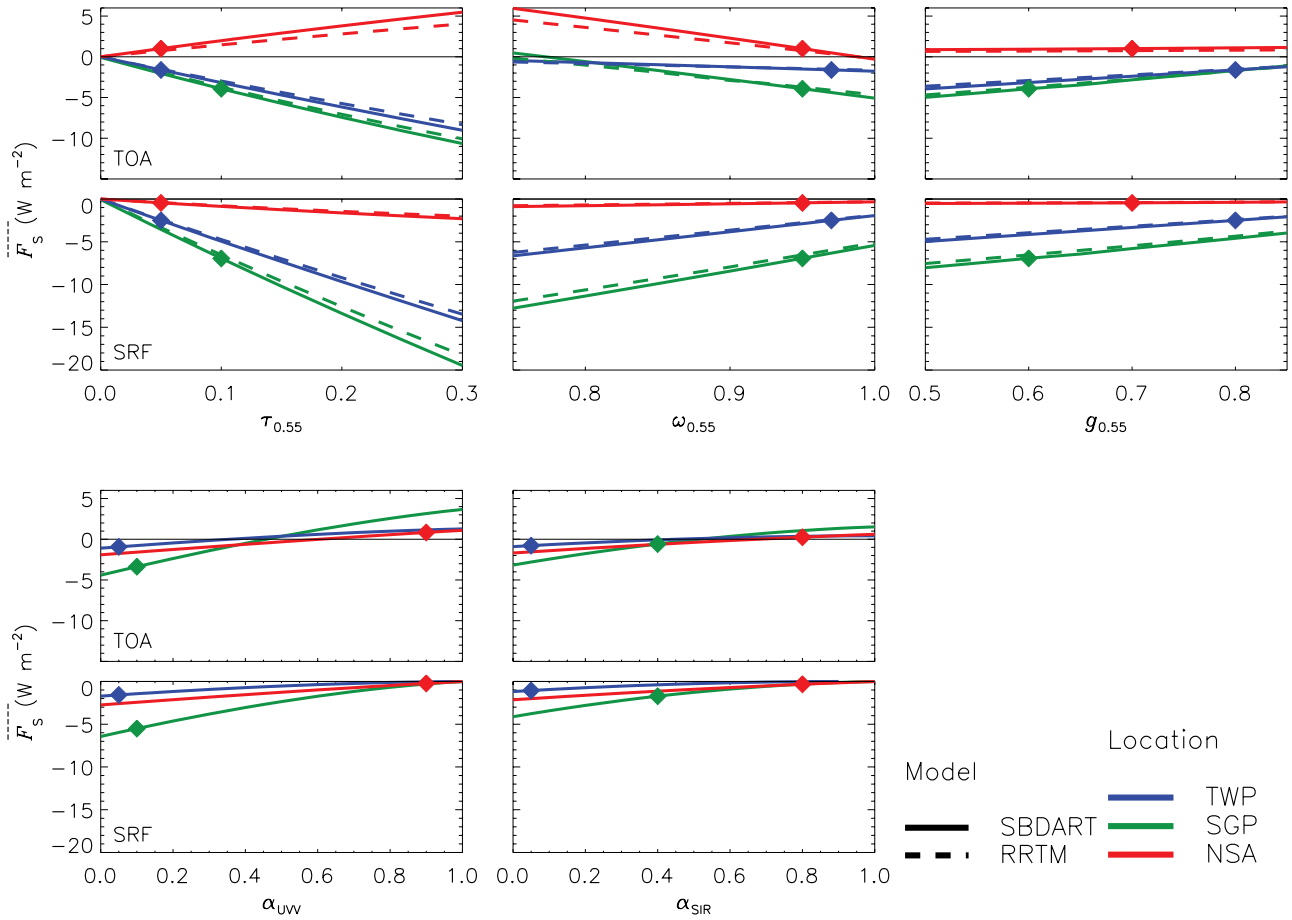

Figure 3a. Dependence of $\overline{F_S}$ (forcing integrated over the solar spectrum and averaged over solar zenith angle for 24 hours at the equinox) on indicated aerosol optical properties and surface albedo as calculated with the SBDART and RRTM models. Symbols denote base case values of the indicated parameters. For each aerosol property the upper panel denotes the forcing at the top of the atmosphere (TOA) and the lower panel at the surface (SRF). The two models are distinguished by the line code; SBDART results are shown with a solid line, and RRTM results, where available, with a dashed line.

quantity to the controlling property depends only weakly on the value of the property. In contrast, the forcings vary nonlinearly with surface albedo, and hence the specific value of α within the range of 0.0–1.0 affects the extent to which it determines variability in a forcing.

[41] The differences in the magnitudes of the several forcings and their dependence on controlling properties among the different sites illustrate how the radiative environment (solar geometry, surface albedo, and atmospheric profile) affects these forcings and their response to uncertainty in the controlling properties. For each radiative quantity the magnitude of forcing is greatest at SGP, primarily because of the higher aerosol optical depth specified for the base case at that site.

[42] At the surface at NSA, variation of each forcing quantity is low overall because of low solar zenith angle, high surface albedo, and low aerosol optical depth. While changes in the TOA forcing at NSA are driven by changes in aerosol optical depth and single scattering albedo, it is effectively insensitive to variation in asymmetry parameter. This is due in part to low insolation and in part to a base case surface reflectance that is similar to the aerosol reflectance. The weak sensitivity of forcing to g and the strong dependence on ω at NSA is due to the high value of α, which results in multiple reflections between the ground and the aerosol, and for even a slightly absorbing aerosol results in positive forcing (warming). Conversely, the asymmetry parameter is a significant driver of variability in SRF forcing at TWP and SGP, sites with a lower base case surface albedo.

[43] Another notable difference among the different locations is the occurrence of positive forcing, principally at the TOA over high surface albedo owing to snow cover, which occurs for the base case at NSA and episodically at SGP but not at TWP. Positive forcing also occurs at the low range of single scattering albedo shown here but only for the solar spectrum average.

[44] The primary difference among the radiative forcing quantities is in the magnitude of the forcing. The magnitude of the instantaneous forcing, $F_S(\theta)$, is greater that that for the diurnally averaged forcing, $\overline{F_S}$, largely because of the lack of forcing at night. The differences in the magnitudes of forcing produce differences in the sensitivity and uncertainty values as discussed below.

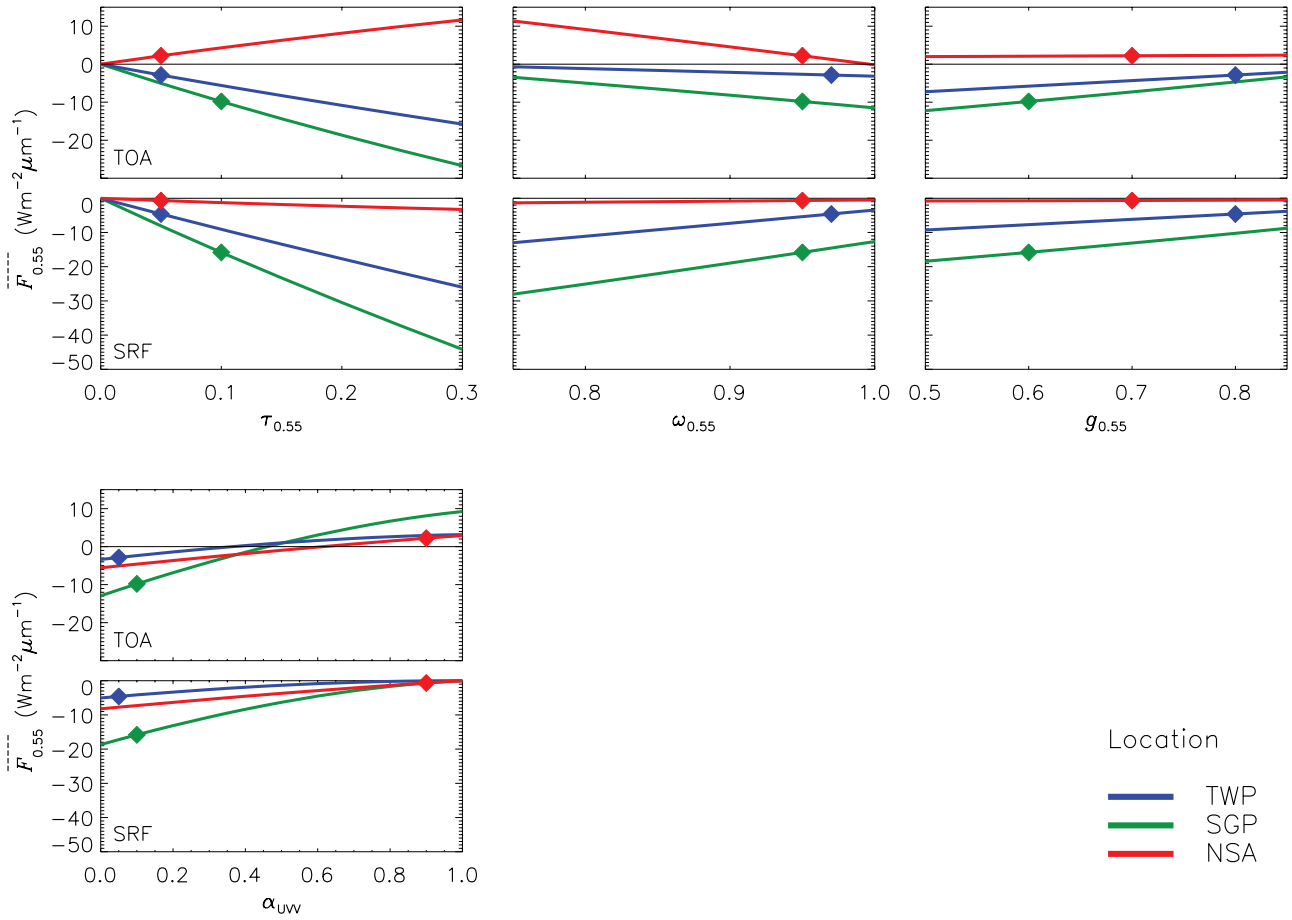

Figure 3b. Dependence of $\overline{F_{0.55}}$ (forcing at 0.55 μm averaged over solar zenith angle for 24 hours at the equinox) on indicated aerosol optical properties and surface albedo as calculated with model. Symbols denote base case values of the indicated parameters. For each aerosol property the upper panel denotes the forcing at the top of the atmosphere (TOA) and the lower panel at the surface (SRF).

[45] The sensitivities of forcings to τ, ω, g, and α for each of the three locations shown in Figure 4 are equal to the slopes in $\overline{F_S}$, $\overline{F_{0.55}}$, and $F_S(\theta)$ with respect to the indicated properties shown in Figures 3a–3c evaluated at the base case for each parameter. The results for the sensitivity calculations for the two models were not substantially different so values of S_i are presented only for the SBDART model. Sensitivities are generally higher at SGP because of the greater aerosol optical depth prescribed for this location and lowest at the SRF at NSA because of the overall low magnitude of the forcings there. The strongest sensitivities are exhibited by the controlling properties τ and ω, with the sensitivities to g and α secondary and of comparable importance to each other, depending on the location and forcing quantity. An exception is the sensitivity to g at the TOA at TWP, which is as strong as or stronger than the sensitivity to ω. For both τ and ω at the TOA, as well as for τ at the SRF, an increase in the value of the property results in increased cooling, while all other sensitivities are positive.

5.2. Uncertainty of Forcing

[46] The sensitivities presented in the previous section indicate the potential contribution of uncertainty in any particular property to the total uncertainty in one of the forcing quantities. For a property with a large sensitivity, if the value of a particular property is well known, its contribution to the uncertainty in F will be low, whereas if the value is not well known the uncertainty in the property may contribute appreciably to uncertainty in forcing. For a property with a small sensitivity, the property will contribute less to uncertainty in forcing regardless of how well the property in known. The sensitivities together with the estimated uncertainties from Table 2 are used to quantify the contribution of each property to the total uncertainty in F. The uncertainty values (equation (3)) for the TOA and SRF for each radiative quantity, as well as the resulting ΔF from equation (4), are presented in Figure 5. Values of the total uncertainty and of the fractional uncertainties with respect to the base case forcings are presented in Table 4.

[47] In most situations, uncertainty in forcing owing to uncertainty in single scattering albedo is greater than for other properties. Exceptions occur, for instance, at TWP at the TOA where the asymmetry parameter is the primary contributor over the low albedo ocean surface. Also, at the surface at NSA absolute uncertainties are low because of the low magnitudes of the several forcings and sensitivities.

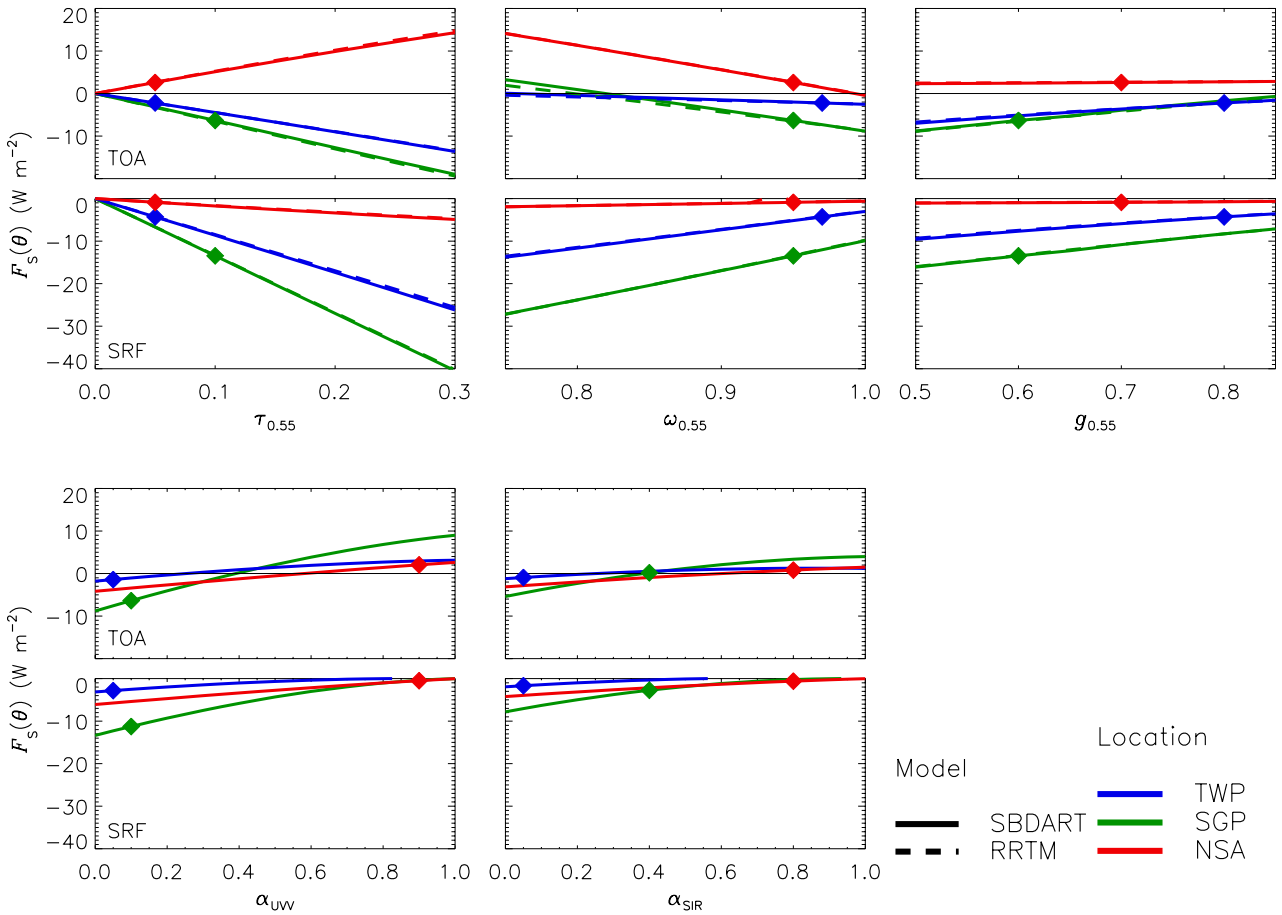

Figure 3c. Dependence of $F_S(\theta)$ (integrated over the shortwave at 30°, 45°, and 70° solar zenith angle for the three sites) on indicated aerosol optical properties and surface albedo as calculated with the SBDART and RRTM models. Symbols denote base case values of the indicated parameters. For each aerosol property the upper panel denotes the forcing at the top of the atmosphere (TOA) and the lower panel at the surface (SRF). The two models are distinguished by the line code; SBDART results are shown with a solid line, and RRTM results, where available, with a dashed line.

Here, the principal contributor to the uncertainty is the uncertainty in UVV surface albedo, especially for the forcing in the narrowband visible. Total uncertainties are highest at SGP, which, again, is a consequence of the greater aerosol optical depth for the base case at this site. In general, uncertainties are lowest for NSA, especially at the surface, where the aerosol has a weak radiative impact over the high albedo surface.

[48] Total absolute uncertainties for most cases are high, up to 1.3 W m^{-2} for $\Delta\overline{F_S}$, and 3 W m^{-2} for $\Delta F_S(\theta)$. Moreover even the lowest absolute uncertainties, 0.2 W m^{-2} for $\Delta\overline{F_S}$, and 0.4 W m^{-2} for ΔF_S (θ), which occur at the surface at NSA, actually produce large relative errors (see Table 4), as the forcing itself is low. Fractional errors are large at NSA in general, at both the TOA and the surface, ranging from ~20 to 80% for all cases addressed here. Examination of the patterns in the uncertainty values indicates that efforts placed on improving the measurement uncertainty in single scattering albedo will have the largest impact on reducing total uncertainty in most cases. In specific cases, however, reduction of measurement uncertainties in asymmetry parameter and surface albedo will have a greater impact in reduction of the total uncertainty. Obtaining accurate TOA forcing estimates for sites such as NSA with high surface albedo and low solar zenith angles requires specific attention to single scattering albedo. It is important to note that the absolute uncertainties owing to other properties will increase as the aerosol optical depth increases.

5.3. Model Comparisons

[49] Various approaches to radiative transfer modeling have resulted from efforts to optimize particular aspects of models such as spectral resolution, reduction in required computational resources, different treatments of successive scattering of radiation, and different representations of the scattering phase function. Efforts to create user-friendly interfaces or maximize flexibility in model inputs have also broadened approaches to modeling. These different approaches ultimately result in a spread among model outputs for the same environmental conditions [*Michalsky et al.*, 2006]. The source of this spread may be a function of

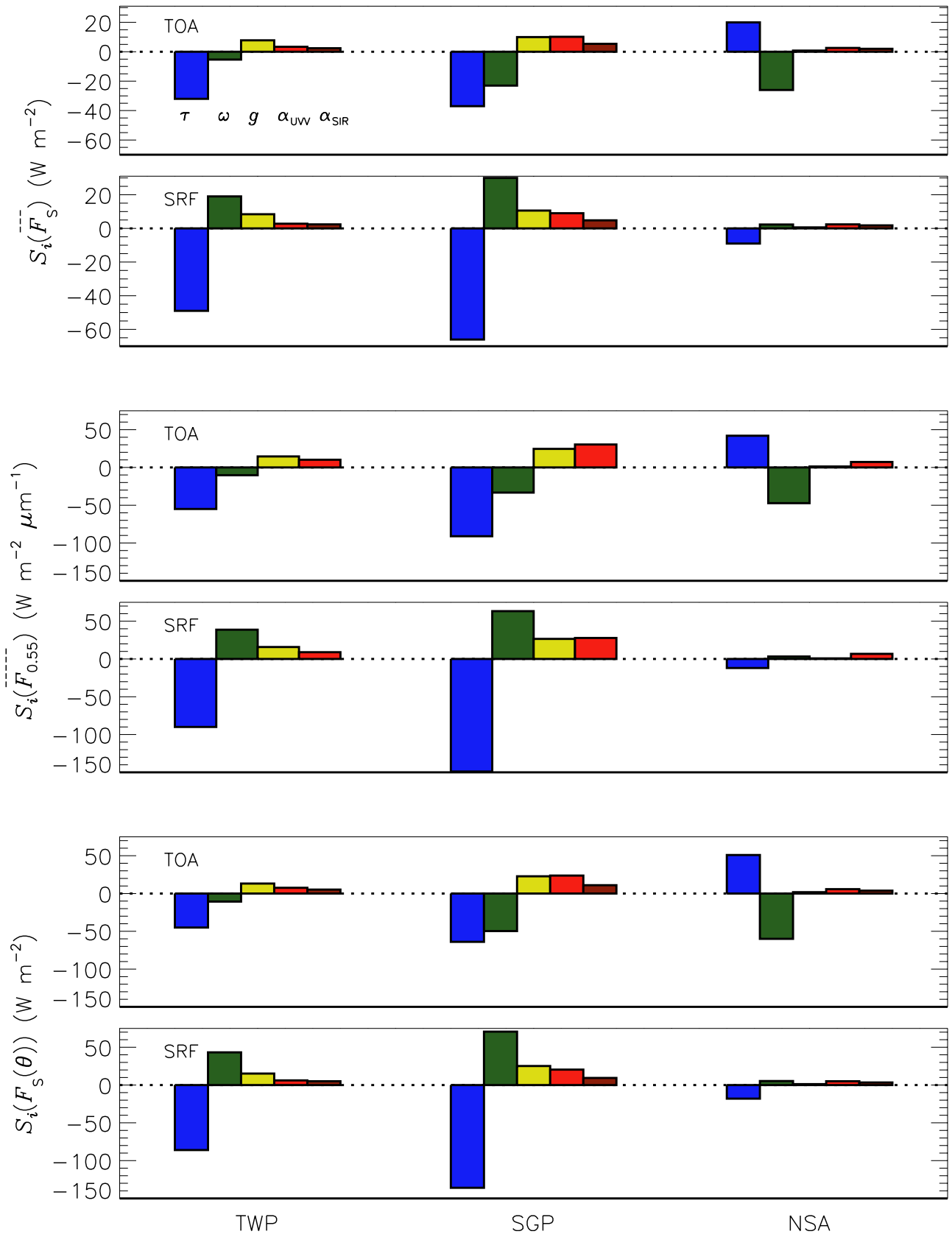

Figure 4. Sensitivities of the forcings ($S_i = \partial F/\partial p_i$) to controlling properties $p_i = \tau$, ω, g, and α for each location and forcing quantity. S_i is presented only for the SBDART model. Sensitivities are per-unit changes in the indicated property. Properties are labeled in the top panel and follow the same pattern throughout the figure.

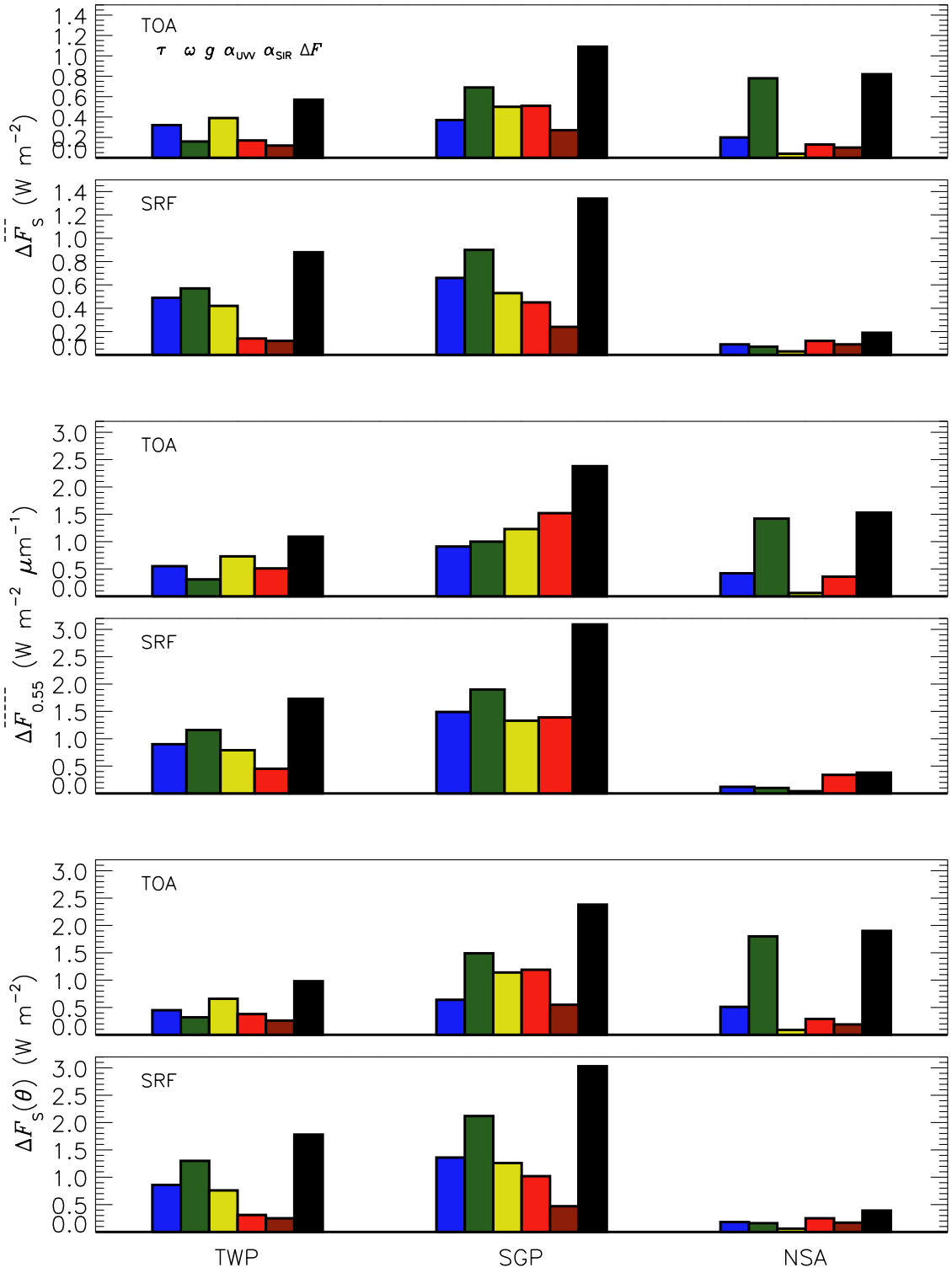

Figure 5. Contribution to uncertainty in each of the several forcings at the top of atmosphere and surface (ΔF_i) owing to uncertainty in each of the several controlling properties τ, ω, g, and α (colored bars); uncertainties in the forcings (ΔF) are denoted by black bars. ΔF_i and ΔF are presented only for the SBDART model. Properties are labeled above in the top panel and follow the same pattern throughout the figure.

Table 4. Absolute and Fractional Total Uncertainties in Forcings Resulting From Uncertainties in Controlling Properties[a]

	TOA			SRF		
	TWP	SGP	NSA	TWP	SGP	NSA
Base case $\overline{F_S}$, W m^{-2}	−1.6	−3.9	1.0	−2.5	−6.9	−0.5
$\Delta\overline{F_S}$, W m^{-2}	0.6	1.1	0.8	0.9	1.3	0.2
Fraction, %	35	28	80	35	19	42
Base case $\overline{F_{0.55}}$, W m$^{-2}\mu$m^{-1}	−2.9	−9.8	2.2	−4.6	−15.8	−0.7
$\Delta\overline{F_{0.55}}$, W m$^{-2}\mu$m^{-1}	1.1	2.4	1.5	1.7	3.1	0.4
Fraction, %	38	24	69	38	20	57
Base case $F_S(\theta)$, W m^{-2}	−2.2	−6.3	2.6	−4.3	−13.5	−0.9
$\Delta F_S(\theta)$, W m^{-2}	1.0	2.4	1.9	1.8	3.0	0.4
Fraction, %	44	38	73	41	23	44

[a]Results are from the SBDART model.

a chosen computational approach that is hardwired into the model or to choices regarding "second-order" model inputs made by the user. (First-order inputs might be considered to be the aerosol optical properties and surface albedo, as examined in this paper; second-order inputs might include the choice in solar spectrum, aerosol phase function, vertical distribution of aerosol density, or water vapor profile.) It is important to understand the contribution of different modeling approaches to uncertainty estimates in calculated forcing. In this paper the importance of model differences to uncertainties in calculated forcings is examined by comparison of SBDART and RRTM results, shown in Figures 3a and 3c and summarized for the sensitivity values in Table 5. The primary differences between these two models, as discussed in section 4, are in their spectral resolution and profiles of aerosol extinction.

[50] Relative differences in sensitivities calculated by the two models are quite low, although in specific cases model error may contribute appreciably to uncertainty in calculated forcing. The differences in computed fluxes between the models are greatest at very low single scattering albedo ($\leq$0.8). Absolute model differences for the sensitivity do not exceed $\sim$6 W m^{-2} per-unit change in the controlling property. In some cases these larger absolute values are a small percentage of the total sensitivity. Larger differences for the diurnally averaged broadband forcing, $\overline{F_S}$, than for the instantaneous broad band forcing, $F_S(\theta)$, are perhaps due to a different scheme for diurnal averaging between the two models; this averaging was performed as a postprocessing routine after the fluxes were calculated from both models for several solar zenith angles.

[51] Results from these full radiative transfer models are compared here to those obtained with the simple analytical model introduced above. The several sensitivities are evaluated for each of the three sites (Table 3) and the results for $F_S(\theta)$ are compared (Table 6) to those obtained with SBDART. The value of the surface albedo is taken as α_{UVV}, as this applies for the region of the spectrum that provides the dominant contribution to the forcing (Figure 1, top panel). The atmospheric transmittance above the aerosol layer, assumed to be due to Rayleigh scattering alone, is approximated by the average of $\exp[-\tau_R(\lambda)\sec\theta]$ over the solar spectrum, where $\tau_R(\lambda)$, the Rayleigh optical depth, is approximated by $(0.3\ \mu m/\lambda)^4$. Values of β and $\partial\beta/\partial g$ used here are estimated from *Wiscombe and Grams* [1976, Figure 3], for which a Henyey-Greenstein phase function was assumed.

[52] The values obtained by this simple model are in fairly good agreement with those from the full radiative transfer model SBDART for TWP and NSA, but not as good for SGP. Two factors previously noted that lead to error in the simplified model include the omission of the wavelength dependence of the aerosol and surface properties and lack of treatment of multiple scattering as aerosol optical depth increases [*Wendisch et al.*, 2001], the latter a possible explanation for the diminished agreement at SGP. The values of single scattering albedo ω for TWP and SGP are well greater than the critical value of this quantity, ω_c, that demarcates positive and negative forcing, implying negative forcing (cooling), whereas for the high surface reflectance at NSA the critical value ω_c approaches unity, and the forcing is positive (warming), implying that absorption by aerosols provides the overwhelmingly dominant contribution to the forcing because of multiple scattering between the surface and the aerosol layer resulting from the high surface albedo.

6. Conclusions

[53] Uncertainty in direct aerosol radiative forcing contributes substantially to uncertainty in estimates of total climate forcing and, in turn, to uncertainty in estimates of climate sensitivity and prediction of climate change. An accurate characterization of the forcing owing to aerosol at a given time and location, such as at ARM sites, is particularly important for the purpose of establishing the accuracy with which radiation can be modeled at such sites by comparison with measurements. The accuracy of such modeled forcing depends on measured aerosol and environmental properties, including their dependencies on wavelength, and on the uncertainties in these values. Here we have examined the sensitivities of calculated aerosol radiative forcing to these properties and have provided estimates

Table 5. Absolute, W m^{-2} per-Unit Change in Controlling Property and (Fractional) Differences Between Sensitivities Calculated With SBDART and RRTM Models (SBDART-RRTM), Evaluated at the Base Case for the Several Forcing Quantities and Locations, at the Top of Atmosphere and Surface

	TOA			SRF		
	TWP	SGP	NSA	TWP	SGP	NSA
S_τ ($\overline{F_S}$)	−3.0 (9%)	−2.0 (5%)	6.0 (30%)	−3.0 (6%)	−3.0 (5%)	−1.0 (11%)
S_ω ($\overline{F_S}$)	−1.0 (19%)	−4.3 (19%)	−6.3 (24%)	1.3 (7%)	2.0 (7%)	0.3 (14%)
S_g ($\overline{F_S}$)	0.8 (10%)	0.4 (4%)	0.2 (25%)	0.6 (7%)	0.2 (2%)	0.2 (33%)
S_τ ($F_S(\theta)$)	−1.0 (2%)	1.0 (2%)	−1.0 (2%)	−1.0 (1%)	−2.0 (2%)	−2.0 (11%)
S_ω ($F_S(\theta)$)	−2.0 (19%)	−5.7 (11%)	−0.3 (1%)	0.3 (1%)	−1.0 (1%)	−0.3 (6%)
S_g($F_S(\theta)$)	0.6 (5%)	−0.8 (4%)	0.6 (33%)	0.6 (4%)	−0.1 (4%)	0.0 (0%)

Table 6. Inputs and Results for a Simple Model of Aerosol TOA Forcing[a]

Quantity	TWP	SGP	NSA
θ	30°	45°	70°
β	0.06	0.17	0.24
$\partial\beta/\partial g$	−0.3	−0.5	−0.6
T_{atm}^2	0.69	0.67	0.55
τ	0.05	0.1	0.05
ω	0.97	0.95	0.95
g	0.8	0.6	0.7
α	0.05	0.1	0.9
ω_c	0.65	0.59	0.9987
F	−2 (−2.2)	−11 (−6.3)	+3 (+2.6)
$\partial F/\partial\tau$	−47 (−45)	−110 (−64)	+66 (+51)
$\partial F/\partial\omega$	−7 (−11)	−31 (−50)	−68 (−60)
$\partial F/\partial g$	+12 (+13)	+35 (+23)	+0.2 (+2)
$\partial F/\partial\alpha$	+8 (+8)	+36 (+24)	+6 (+6)

[a]Values in parentheses are the results from SBDART for $F_S(\theta)$. Unit of forcing, F, W m^{-2}; unit of sensitivities, dF/dp_i, W m^{-2} per-unit change in controlling property.

of uncertainties for different locations and modeling scenarios to provide a reference and a framework for improving accuracy in determining aerosol forcing for a range of applicable conditions.

[54] Given the values for measurement uncertainties used in this study, uncertainty in the total modeled forcing is high, ranging from approximately 20 to 80%, corresponding to a range of 0.6 to 1.1 W m^{-2} at the TOA and 0.2 to 1.3 W m^{-2} at the surface for local diurnally averaged forcing for typical aerosol and environmental conditions at the three sites. For local instantaneous forcing, uncertainty in the total modeled forcing ranges from approximately 20 to 70%, corresponding to a range of 1 to 2.4 W m^{-2} at the TOA and 0.4 to 3 W m^{-2} at the surface. Uncertainty in the total modeled forcing for narrowband forcing also ranges from approximately 20 to 70%, corresponding to a range of 1.1 to 2.4 W m^{-2} μm^{-1} at the TOA and 0.4 to 3.1 W m^{-2} μm^{-1} at the surface. Achieving estimates of aerosol DRF with an acceptable level of uncertainty for climate modeling applications requires reduction in the total uncertainty to a fraction of current values for most of the cases presented here. An examination of the contributions of the several controlling properties to uncertainty in DRF indicates that the primary area for improvement is in the measurement of the single scattering albedo, followed by improvements in the measurement of the asymmetry parameter.

[55] It should also be noted that the results of this analysis are dependent on the values chosen for measurement uncertainties of the aerosol and surface properties. These are estimated errors and the actual error for any specific set of measurements may be quite different, depending on the instrumental and sampling approaches, as well as on the state of the atmosphere. In comparing broadband to spectral calculations, the differences will also depend on the wavelength dependencies assumed for each property. Those used here are parameterizations representing unknown spectral behavior, for aerosol properties where measurements have not been made, or simplification, for the surface albedo.

[56] Realistically, several criteria must be considered in making decisions on where to place efforts for decreasing measurement uncertainties of these various properties: the extent to which the property drives variation in a given forcing quantity, the current measurement uncertainty in the property, and the potential for appreciable improvements in that measurement accuracy. Despite its low fractional uncertainty, the low absolute uncertainty in aerosol optical depth still contributes substantially to total uncertainty in the several forcing quantities. While incremental improvements in measurement uncertainty for this quantity would still decrease total uncertainty in the several forcings, substantial reduction from its present value seems unlikely. Thus further efforts spent in reducing this measurement uncertainty may not have as great an impact as focusing on different aerosol properties that have measurement uncertainties that are more easily addressed, for example, the single scattering albedo. Likewise, knowledge of the asymmetry parameter may be of lesser importance to accuracy in calculating forcing than aerosol optical depth, but measurement uncertainties are relatively high and improvements in observations may require less effort and may appreciably enhance accuracy in calculating aerosol forcing.

[57] In addition to the measurement uncertainty, averaging observed properties over space and time to scales that are desired for modeling will introduce additional uncertainty in the resulting estimates of forcing. Where observations are sparse, specification of values for model computations are based on climatology, averaged values over different scales, observations from neighboring regions, or from literature based on an assumed aerosol type. For example, if the variability in a property is observed to be within a particular range, computing the sensitivity over this range permits calculation of the uncertainty owing to the observed variability in the property. If some measure of central tendency is used to represent such a range in a property, the variation from this central measure must be combined with the known or estimated measurement uncertainty to determine the true contribution of this value to uncertainty in the calculated forcing. This can be achieved for a given time period or region of interest by specifying the range of variability in either time or space. Calculation of the contribution to uncertainty in forcing from other sources, such as averaging over varying spatial and temporal domains, for instance, is not considered here, but is straightforward using the present results.

[58] **Acknowledgments.** Special thanks to Joseph Michalsky for his time and valuable input to this project. Funding for this project was provided by the Office of Science (BER), U.S. Department of Energy.

References

Anderson, T. L., et al. (1999), Aerosol backscatter fraction and single scattering albedo: Measured values and uncertainties at a coastal station in the Pacific Northwest, *J. Geophys. Res.*, *104*, 26,793–26,807.

Anderson, T. L., et al. (2003), Climate forcing by aerosols—A hazy picture, *Science*, *300*, 1103–1104, doi:10.1126/science.1084777.

Anderson, T. L., et al. (2005), An "A-Train" strategy for quantifying direct climate forcing by anthropogenic aerosols, *Bull. Am. Meteorol. Soc.*, *86*, 1795–1808.

Bates, T. S., et al. (2006), Aerosol direct radiative effects over the northwest Atlantic, northwest Pacific, and North Indian Oceans: Estimates based on in-situ chemical and optical measurements and chemical transport modeling, *Atmos. Chem. Phys.*, *6*, 1657–1732.

Bellouin, N., et al. (2005), Global estimate of aerosol direct radiative forcing from satellite measurements, *Nature*, *438*, 1138–1141.

Bergstrom, R. W., and P. B. Russell (1999), Estimation of aerosol radiative effects over the mid-latitude North Atlantic region from satellite and in situ measurements, *Geophys. Res. Lett.*, *26*, 1731–1734.

Boucher, O., et al. (1998), Intercomparison of models representing direct shortwave radiative forcing by sulfate aerosols, *J. Geophys. Res.*, *103*, 16,979–16,998.

Charlson, R. J., et al. (1990), Sulphate aerosol and climate, *Nature*, *348*, 22.

Charlson, R. J., et al. (1991), Perturbation of the northern hemisphere radiative balance by backscattering from anthropogenic aerosols, *Tellus, Ser. AB*, *43*, 152–163.

Charlson, R. J., et al. (1992), Climate forcing by anthropogenic aerosols, *Science*, *255*, 423–430.

Chylek, P., and J. Wong (1995), Effect of absorbing aerosols on global radiation budget, *Geophys. Res. Lett.*, *22*, 929–931.

Clough, S. A., et al. (2004), Atmospheric radiative transfer modeling: A summary of the AER codes, *J. Quant. Spectrosc. Radiat. Transfer*, *91*, 233–244.

Delene, D., and J. A. Ogren (2002), Variability of aerosol optical properties at four North American surface monitoring sites, *J. Atmos. Sci.*, *59*, 1135–1150.

Dubovik, O., and M. D. King (2000), A flexible inversion algorithm for retrieval of aerosol optical properties from Sun and sky radiance measurements, *J. Geophys. Res.*, *105*, 20,673–20,696.

Forster, P., et al. (2007), Changes in atmospheric constituents and in radiative forcing, in *Climate Change 2007: The Physical Science Basis—Contribution of Working Group I to the Fourth Assessment Report of the Intergovernmental Panel on Climate Change*, edited by S. Solomon et al., pp. 289–348, Cambridge Univ. Press, New York.

Gueymard, C. A. (2004), The Sun's total and spectral irradiance for solar energy applications and solar radiation models, *Sol. Energy*, *76*, 423–453.

Halthore, R. N., and S. E. Schwartz (2000), Comparison of model-estimated and measured diffuse downward irradiance at surface in cloud-free skies, *J. Geophys. Res.*, *105*, 20,165–20,177.

Halthore, R. N., et al. (2005), Intercomparison of shortwave radiative transfer codes and measurements, *J. Geophys. Res.*, *110*, D11206, doi:10.1029/2004JD005293.

Harrison, L., et al. (1994), Automated multifilter rotating shadow-band radiometer: An instrument for optical depth and radiation measurements, *Appl. Opt.*, *33*, 5118–5125.

Haywood, J. M., and K. P. Shine (1995), The effect of anthropogenic sulfate and soot aerosol on the clear sky planetary radiation budget, *Geophys. Res. Lett.*, *22*, 603–606.

Holben, B. N., et al. (1998), AERONET—A federated instrument network and data archive for aerosol characterization, *Remote Sens. Environ.*, *66*, 1–16.

Intergovernmental Panel on Climate Change (IPCC) (2001), Summary for policymakers, in *Climate Change 2001—The Scientific Basis: Contribution of Working Group I to the Third Assessment Report of the Intergovernmental Panel on Climate Change*, edited by J. T. Houghton et al., Cambridge Univ. Press, New York.

Intergovernmental Panel on Climate Change (IPCC) (2007), Summary for policymakers, in *Climate Change 2007—The Physical Science Basis: Contribution of Working Group I to the Fourth Assessment Report of the Intergovernmental Panel on Climate Change*, Cambridge Univ. Press., New York.

Kassianov, E. I., J. C. Barnard, and T. P. Ackerman (2005), Retrieval of aerosol microphysical properties using surface MultiFilter Rotating Shadowband Radiometer (MFRSR) data: Modeling and observations, *J. Geophys. Res.*, *110*, D09201, doi:10.1029/2004JD005337.

Kato, S., et al. (1997), Uncertainties in modeled and measured clear-sky surface shortwave irradiances, *J. Geophys. Res.*, *102*, 25,881–25,898.

McClatchey, R. A., R. W. Fenn, J. E. A. Selby, F. E. Volz, and J. S. Garing (1972), *Optical Properties of the Atmosphere*, 113 pp., Air Force Cambridge Res. Lab., Hanscom Air Force Base, Mass. (Available at http://stinet.dtic.mil/oai/oai?verb=getRecord&metadataPrefix=html&identifier=AD0753075)

Michalsky, J. J., G. P. Anderson, J. Barnard, J. Delamere, C. Gueymard, S. Kato, P. Kiedron, A. McComiskey, and P. Ricchiazzi (2006), Shortwave radiative closure studies for clear skies during the Atmospheric Radiation Measurement 2003 Aerosol Intensive Observation Period, *J. Geophys. Res.*, *111*, D14S90, doi:10.1029/2005JD006341.

Penner, J. E., et al. (1992), Effects of aerosol from biomass burning on the global radiation budget, *Science*, *256*, 1432–1433.

Penner, J. E., et al. (1994), Quantifying and minimizing uncertainty in climate forcing by anthropogenic aerosols, *Bull. Am. Meteorol. Soc.*, *75*, 375–400.

Penner, J. E., et al. (2001), Aerosols, their direct and indirect effects, in *Climate Change 2001: The Scientific Basis—Contribution of Working Group I to the Third Assessment Report of the Intergovernmental Panel on Climate Change*, edited by J. T. Houghton et al., pp. 129–234, Cambridge Univ. Press, New York.

Redemann, J., et al. (2000), Case studies of the vertical structure of the direct shortwave aerosol radiative forcing during TARFOX, *J. Geophys. Res.*, *105*, 9971–9979.

Redemann, J., P. Pilewskie, P. B. Russell, J. M. Livingston, S. Howard, B. Schmid, J. Pommier, W. Gore, J. Eilers, and M. Wendisch (2006), Airborne measurements of spectral direct aerosol radiative forcing in the Intercontinental chemical Transport Experiment/Intercontinental Transport and Chemical Transformation of anthropogenic pollution, 2004, *J. Geophys. Res.*, *111*, D14210, doi:10.1029/2005JD006812.

Ricchiazzi, P., et al. (1998), SBDART: A research and teaching software tool for plane-parallel radiative transfer in the Earth's atmosphere, *Bull. Am. Meteorol. Soc.*, *79*, 2101–2114.

Russell, P. B., et al. (1997), Aerosol climate effects: Local radiative forcing and column closure experiments, *J. Geophys. Res.*, *102*, 9397–9407.

Russell, P. B., et al. (2007), Multi-grid-cell validation of satellite aerosol property retrievals in INTEX/ITCT/ICARTT 2004, *J. Geophys. Res.*, *112*, D12S09, doi:10.1029/2006JD007606.

Schmid, B., et al. (2006), How well do state-of-the-art techniques measuring the vertical profile of tropospheric aerosol extinction compare?, *J. Geophys. Res.*, *111*, D05S07, doi:10.1029/2005JD005837.

Schmid, B., et al. (2007), The sensitivity of shortwave radiative forcing and heating rates to the aerosol vertical profile, paper presented at Seventeenth ARM Science Team Meeting, Atmos. Radiat. Manage. Program, Monterey, Calif., 26–30 March.

Schulz, M., et al. (2006), Radiative forcing by aerosols as derived from the AeroCom present-day and pre-industrial simulations, *Atmos. Chem. Phys.*, *6*, 5225–5246.

Schwartz, S. E. (2004), Uncertainty requirements in radiative forcing of climate change, *J. Air Waste Manage. Assoc.*, *54*, 1351–1359.

Stamnes, K., et al. (1988), Numerically stable algorithm for discrete-ordinate-method radiative transfer in multiple scattering and emitting layered media, *Appl. Opt.*, *27*, 2502–2509.

Wagener, R., S. Nemesure, and S. E. Schwartz (1997), Aerosol optical depth over oceans: High space- and time-resolution retrieval and error budget from satellite radiometry, *J. Atmos. Oceanic Technol.*, *14*, 577–590.

Wendisch, M., et al. (2001), Measurement-based aerosol forcing calculations: The influence of model complexity, *Meteorol. Z.*, *10*, 45–60.

Wiscombe, W. J., and G. W. Grams (1976), The backscattered fraction in two-stream approximations, *J. Atmos. Sci.*, *33*, 2240–2451.

Yu, H., et al. (2006), A review of measurement-based assessments of the aerosol direct radiative effect and forcing, *Atmos. Chem. Phys.*, *6*, 613–666.

H. Guan, Bay Area Environmental Research Institute, 560 Third Street West, Sonoma, CA 95476, USA. (guan@clio.arc.nasa.gov)

E. R. Lewis and S. E. Schwartz, Atmospheric Sciences Division, Brookhaven National Laboratory, Building 815E, Upton, NY 11973, USA. (elewis@bnl.gov)

A. McComiskey, NOAA Cooperative Institute for Research in the Environmental Sciences, University of Colorado, R/GMD-1, 325 Broadway, Boulder, CO 80305, USA. (allison.mccomiskey@noaa.gov)

J. A. Ogren, NOAA Earth System Research Laboratory, R/GMD-1, 325 Broadway, Boulder, CO 80305, USA. (john.a.ogren@noaa.gov)

P. Ricchiazzi, Institute for Computational Earth System Science, University of California, Santa Barbara, Ellison Hall 3060, Santa Barbara, CA 93106-3060, USA. (paul@icess.ucsb.edu)

B. Schmid, Pacific Northwest National Laboratory, MSIN: K9-24, 902 Battelle Boulevard, P.O. Box 999, Richland, WA 99352, USA. (beat.schmid@pnl.gov)